

Plasma polypyrrole micro-coatings on metallic stents

Lidia M. Gómez^{1,3} · M. Guadalupe Olayo¹ ·
V́ctor Sánchez-Mendieta³ · Maribel González-Torres^{1,3} ·
Francisco González-Salgado^{1,4} · Rodrigo Mondragón Lozano¹ ·
Rafael Basurto² · Guillermo J. Cruz¹

Received: 21 January 2016 / Revised: 15 July 2016 / Accepted: 29 July 2016 /
Published online: 4 August 2016
© Springer-Verlag Berlin Heidelberg 2016

Abstract Stainless steel stents were coated with biocompatible polypyrrole doped with iodine and synthesized by plasma to add a polymeric layer on the metallic surfaces that may reduce some implant rejection reactions in the human circulatory system due to the implantation of metallic surfaces. Trying to increase the adhesion in the polymer–metal interface, this study used erosion, oxidation and sensitization of the metallic stents with an in situ posterior polymerization of the monomer. All processes were carried out by plasma which increased the reactivity of the metallic surfaces producing chemical bonds between polymers and stents with a high possibility to resist the blood conditions without peeling or detachment that may expose the metallic surface to the blood. The results showed that the coatings contain pyrrole rings joined among them in different configurations which originated crosslinked polymers. The erosion did not change, substantially, the density of protrusions, but changed only their width and height, and the coatings acquired the morphology of the metallic surface with a 3.7 nm roughness and protrusion separation of 35.6 nm. The coated stents were immersed in phosphate-buffered saline (PBS) solutions with pH \sim 7.4 at 37 °C to partially simulate the chemical conditions in arteries and veins, in which the coating remained adhered on the stent up to 2 months without significant degradation. The immersion in PBS static fluids

✉ Guillermo J. Cruz
guillermo.cruz@inin.gob.mx; guillermoj.cruz@hotmail.com

- ¹ Departamento de Física, Instituto Nacional de Investigaciones Nucleares, Carretera México-Toluca, Km. 36.5, CP 52750 Ocoyoacac, Estado de México, Mexico
- ² Departamento de Química, Instituto Nacional de Investigaciones Nucleares, Carretera México-Toluca, Km. 36.5, CP 52750 Ocoyoacac, Estado de México, Mexico
- ³ Posgrado en Ciencia de Materiales, Facultad de Química, Universidad Autónoma del Estado de México, Paseo Tollocan esq. Paseo Colón, CP 52000 Toluca, Estado de México, Mexico
- ⁴ Departamento de Posgrado, Instituto Tecnológico de Toluca, Av. Tecnológico s/n, Col. La Virgen, CP 52140 Metepec, Estado de México, Mexico

caused a roughness decrease from 3.7 to 2.4 nm with a protrusion separation of 35.4 nm, however, in PBS dynamic fluids, the erosion increased the roughness and protrusion separation up to 9.3 and 43.9 nm, respectively.

Keywords Stents · Polypyrrole · Coatings · Plasma · XPS

Introduction

A stent is a cylindrical metallic mesh of a few millimeters diameter which is implanted in the circulatory system to enlarge the cross-sectional area of partially obstructed veins or arteries to restore the blood flow. However, the metallic surface usually causes rejection reactions that produce again, at mid-term, clots and re-obstructions in the circulatory system [1]. To prevent this secondary obstruction after the implantation, some stents have been covered with biocompatible materials as anti-coagulants, anti-inflammatory and anti-proliferative drugs [2, 3]. The coated stents have resulted with less secondary effects than the uncoated ones, but the re-obstruction is always present, due, among other reasons, to partial detachment of the coatings under the constant blood flow and to the physicochemical attack of blood, both effects produce corrosion and release of noxious metal ions and other particles to the blood flow. To reduce these problems, the biocompatible coatings should withstand the blood flow on the stents for long periods [4]. However, the bonding between polymers and metals is a difficult task, because both phases have different characteristics and properties.

One of the polymers used as coatings to protect metals against corrosion is polypyrrole (PPy), many polymerization techniques have been used in that task, such as electrochemistry, plasma, and sonication [5–8]. Wang and Northwood coated stainless steel with PPy using galvanostatic methods and found that the metallic corrosion decreased up to ten times with the coating [9]. De Jesus and collaborators used sensitization with water and argon erosion to improve the adhesion between PPy synthesized by plasma with nitinol and stainless steel (SS) substrates. The coated metals were immersed for 24 h in a phosphate-buffered saline (PBS) solution with salt concentration and pH similar to the blood observing that the coatings on nitinol were bonded stronger than onto SS [10]. Khan and collaborators electropolymerized polypyrrole-*N*-succinimidyl ester on SS and encountered that it is more biocompatible than the uncoated metal [11].

The main problem of the polymeric coatings on metals is the detach of the soft layers in contact with fluids, static or in movement [12, 13]. To reduce this problem, this work used consecutively erosion, oxidation and polymerization of pyrrole by plasma directly on the metallic surface of a stent to cover the twisted segments of an SS stent with an iodine-doped polypyrrole (PPy/I) micro-coating. Static and dynamic fluid models were used to test the union between the stent and PPy/I under total immersion during 2 months.

Materials and methods

SS stents (Arthesys, France) were coated with PPy synthesized and doped with iodine by plasma in a vacuum tubular glass reactor of 1200 cm³ with electrodes and stainless steel flanges at the ends. The vacuum system includes a 2015 C1 Alcatel Pascal vacuum pump, a 25LNTS Alcatel liquid-nitrogen condenser and a 945 MKS Instruments pressure gauge Pirani HPSTM. Pyrrole (Aldrich, 98 %), iodine (Aldrich, 99.8 %) and hydrogen peroxide (RAB) were settled in sealed containers with volume of approximately 90 mL and introduced separately into the reactor in gas phase.

The stents were subjected to an initial wash with water and soap in sonic bath for 15 min and to another cleaning with acetone (JT Baker, 99.6 %) to remove grease. Later, they were placed in the reactor, on the electrode connected to the RF output of a VM1000A Dressler Cesar power supply, to erode and oxidize with of Ar and H₂O₂ plasmas. Electrical glow discharges were set at 13.56 MHz, 100 W and 10⁻¹ mbar during 45 min for Ar and H₂O₂. Then, the coating was synthesized on the sensitized surface with pyrrole and iodine plasma at 10⁻¹ mbar and 20 W during 10 min.

Scanning electron microscopy (SEM) was performed using a JEOL JSM-5900LV apparatus to observe the morphology of the stents and PPy/I-coatings and to test the integrity of the polymeric coating after the immersion. Atomic force microscopy (AFM) was carried out using a Cypher Asylum Research microscope to study the morphology of the uncoated stent and PPy/I-coatings. The resistance of the coatings was evaluated by immersion in PBS solutions (in mM: NaCl = 24, Na₂HPO₄ = 10, KH₂PO₄ = 3) at 37 °C during 2 months in static and dynamic fluids, simulating the average velocity (77.2 cm/s) of an artery diameter = 12.6 mm, that corresponds at a cardiovascular system of a typical adult human of 70 kg [14]. Surface chemical analyses of the metallic substrates and polymeric coatings were studied by X-ray photoelectron spectroscopy (XPS) with an Al monochromatic Thermo K- α spectrometer. The analysis area was approximately 50 μ m diameter on one of the external faces of the stent curved wires. It is important to remark that the polymeric layer is a micro-coating that cannot be tested by ordinary macro methods.

Results and discussion

Morphology of substrates

The morphology of uncoated stents used in this work taken by SEM is shown in Fig. 1. Figure 1a shows the global profile of the stent, 17 mm length and 1.5 mm diameter. It is made of straight and curved sections of rectangular wires of approximately 50 μ m thickness and 100 μ m width bent in different directions, see Fig. 1b. Some bending tracks on the plain surface can be seen in the micrographs, probably due to the manufacturing process, see Fig. 1c.

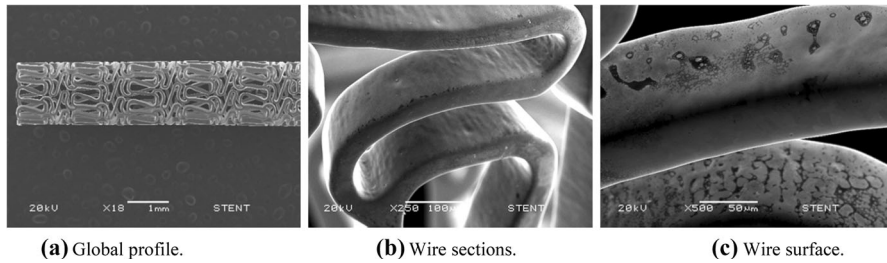


Fig. 1 SEM micrographs of uncoated SS stents at $\times 18$, $\times 250$ and $\times 500$ magnifications

Figure 2 shows the stent surface at a higher magnification taken by AFM. Figure 2a shows 2D images and Fig. 2b shows 3D images. The stent plain wire surface has light scratches and protrusions with root mean square roughness (R_{rms}) of approximately 3.1 nm, Fig. 2b, the bending tracks are not considered as protrusions, because they involve a bigger area than that considered in the general protrusions.

Coating morphology

The coating morphology in different perspectives is presented in Fig. 3, which shows that the coating follows the surface and there are no signs of detachment indicating good adhesion. The irregularities on the surface were covered with the polymeric coating leaving a macro-smoother surface. As the plasma erosion, sensitization and polymerization were carried out in gas phase, and it is possible that the organic layers inside the voids were removed and the polymeric layers were attached in the same way as on the other surfaces, even on the hidden twisted corners of the stent, see Fig. 3a. The coating covered homogeneously inside and outside the stent channel, because the complete stent was polarized and the movement of ions was around the whole metallic surfaces. However, some irregularities appeared on the wire surface in the form of some small polymer particles on the coating surface that do not affect the coating greatly, see Fig. 3b.

AFM images and roughness of PPy/I-coatings surfaces are shown in Fig. 4. The coating follows the surface and increases, lightly, the protrusions on the substrate. The R_{rms} of PPy/I-coatings on the stent is 3.7 nm (Fig. 4b), however, although the mean roughness of the coating is much bigger than that of the naked metallic surface, the polymeric protrusions are much softer than the metallic ones.

Immersion in PBS solutions

In the case of implants in the human body, time is critical because many processes trigger after the implant [15]. For this reason, the polymer–metal adhesion was evaluated during 2 months in which the re-obstruction of veins and arteries has been reported [16]. If the stent retains the biocompatible polymeric layer, it may be accepted for much longer time preventing the re-obstruction of the circulatory system [2]. To simulate the conditions after the implantation, the coatings were

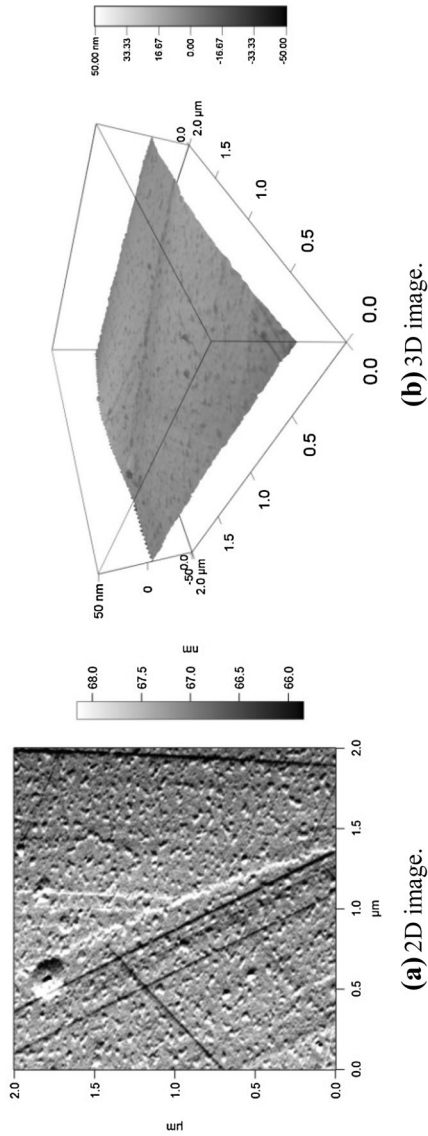


Fig. 2 AFM images of uncoated SS stents, approximately $\times 50,000$ magnification. Area $4 \mu\text{m}^2$

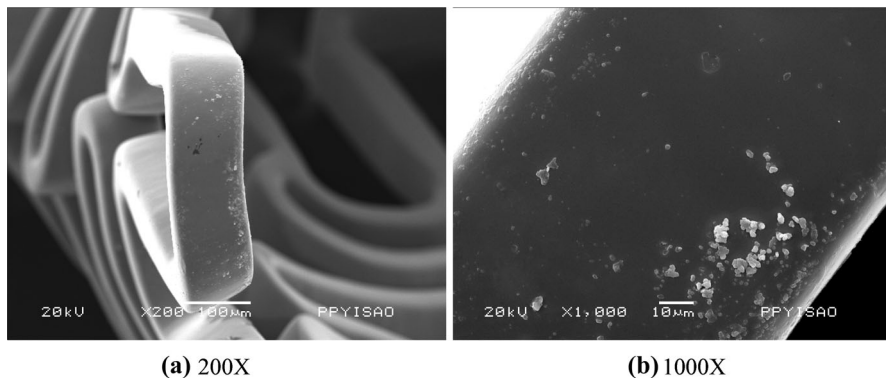


Fig. 3 Different views of the PPy/I-coatings on SS stents

immersed in PBS solutions at 37 °C using static and dynamic fluids. In both models, the stent was suspended in the middle of the fluids to test their effect inside and outside the stent channel. The integrity of the coating was evaluated visually using scanning electron microscopy, see different views of the stent in Fig. 5. The results indicated that after 2 months, the coatings remained adhered to the metal in contact with the PBS solution on all faces.

Figure 6 shows AFM images and roughness of PPy/I-coatings surfaces after 2 months in PBS solution in static and dynamic fluids, Fig. 6a, b, respectively. The coating in dynamic fluids shows greater protrusions ($R_{\text{rms}} = 9.3$ nm, Fig. 6b, right) than the coating in static fluids ($R_{\text{rms}} = 2.4$ nm, Fig. 6a, right). The interaction of the solution in the dynamic model caused inhomogeneous removal of the superficial polymeric layers producing the roughness difference between the two models.

The height and separation of protrusions were studied with a normal distribution function. 545 height protrusions and 100 distances between protrusions were measured, see Fig. 7. The maximum height protrusions of stent and PPy/I-coating were found in 10.9 and 16.6 nm, respectively (Fig. 7a). On the other hand, the distance interval between protrusions was 10.1–100.3 nm and 6.9–121.1 nm on the stent and PPy/I-coating, respectively (Fig. 7b). In the same order, the center of the height distribution is approximately 1.4 and 1.1 nm, and the center of the distance between protrusions was 34.2 and 35.6 nm, respectively. The similitude of distances between protrusions in SS stent and PPy/I-coating shows a homogeneous cover.

The height and separation of protrusion distribution for the static and dynamic models suggest that in the static model, there is a uniform detachment of film. The top height of PPy/I-coating protrusions after 2 months in the static model was located in 19.1 nm with average in 1.8 nm, and the distance between protrusions was 12.0–136.5 nm with average in 35.4 nm. On the other hand, the average height of PPy/I-coating protrusions after 2 months in the dynamic model was 21.55 nm and the average distance between protrusions was 43.9 nm. The data suggest that the fluid velocity of PBS causes separation of several nano-segments on the superficial layers producing an uneven surface compared to the static model.

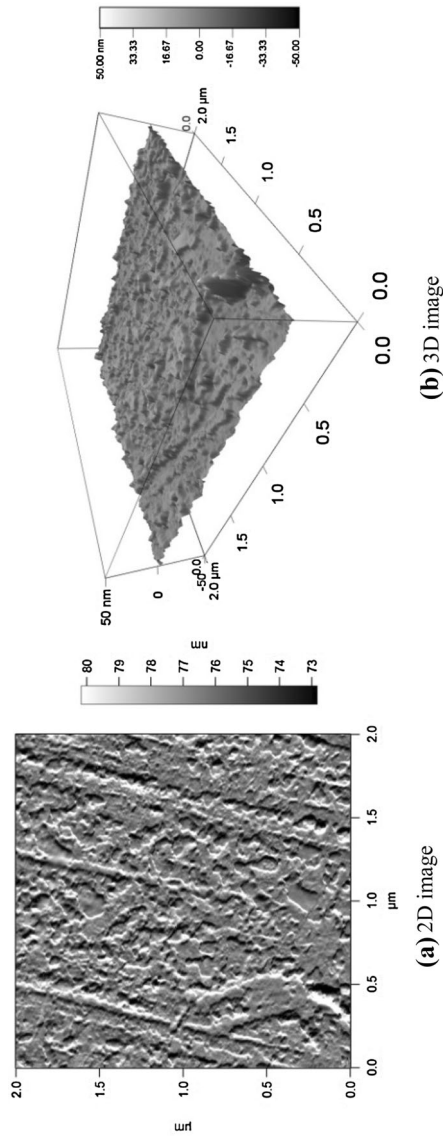
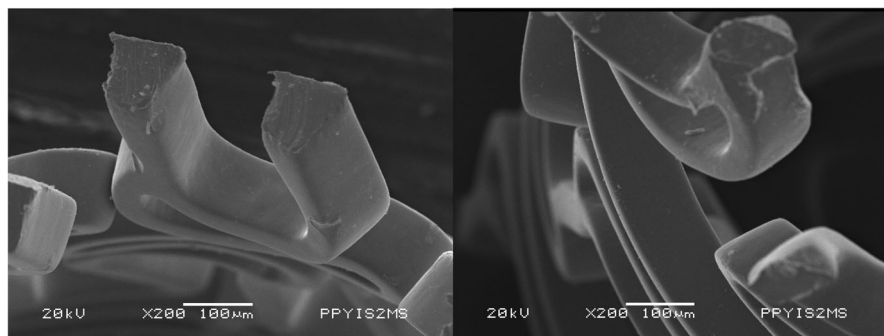
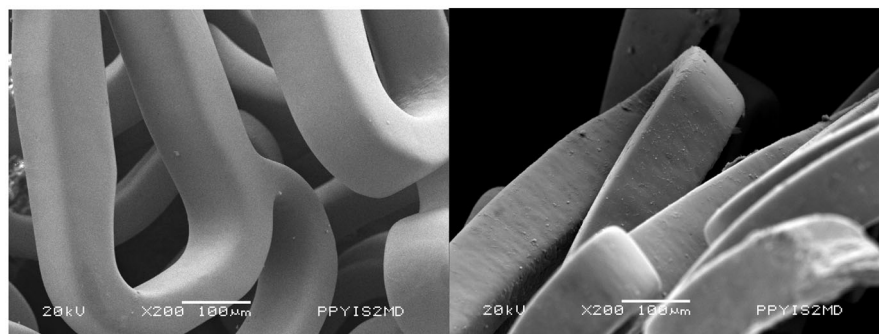


Fig. 4 AFM images of coatings of PPy/I on SS stent. **a** 2D images with Area = $4 \mu\text{m}^2$, approximately $\times 50,000$ and **b** 3D images



(a) Stent in static fluids.



(b) Stent in dynamic fluids.

Fig. 5 SS stent coated with PPy/I after immersion in PBS at 37 °C during 2 months, **a** in static fluids and **b** in dynamic fluids. See the integrity of the polymeric layer, no detachments or peeling can be seen in both cases

Superficial elemental content

Figure 8 shows the XPS survey spectra of the metallic substrates and PPy/I-coatings with the atomic percentage. There are two runs, the surface and an eroded surface with Ar ions during 30 s, which means a depth of approximately 20–30 nm. The only elements detected on the metallic surface without erosion were C, O and Fe, which suggests that the stent surface has a first organic layer of C and Fe oxides, due to the exposure to the atmosphere. After the erosion, the elements detected were O, Cr, Fe, Co and Ni, which are the elements of the SS alloy. Note that the C content on the metallic surfaces reduced to almost zero and that the O content increased after the erosion. These numbers suggest that the organic layer was partially removed from the surface, thus exposing the metallic face.

The main elements found on the PPy/I-coatings without erosion were C, N, O and I. C and N are attributed to the pyrrole structure, O could be attributed mainly to oxidation and I represents the doping. After the erosion, the same elements were detected but with different content. The most important change is a reduction up to 20 % of the O content after the erosion, which can be due to the atmospheric

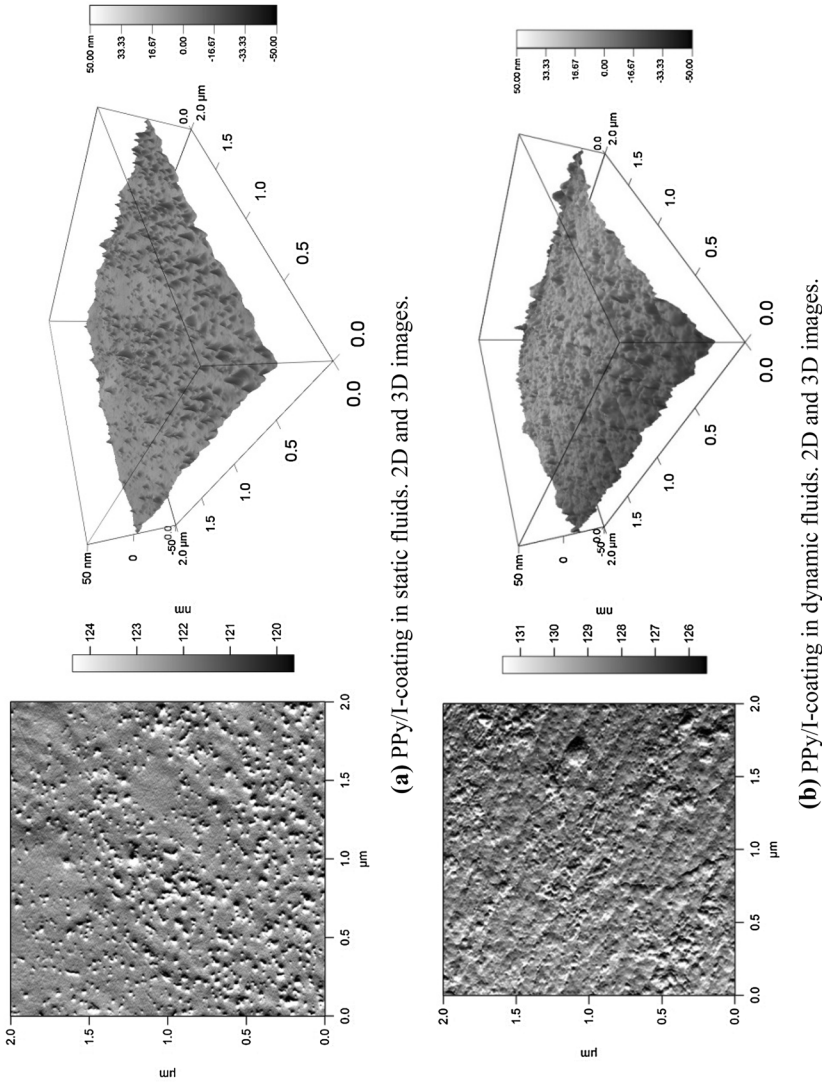


Fig. 6 AFM images of coatings of PPy/I on SS stent after 2 months in PBS at 37 °C, **a** in static fluids and **b** in dynamic fluids. 2D images with area = 4 μm², approximately ×50,000 (*left*) and 3D images (*right*)

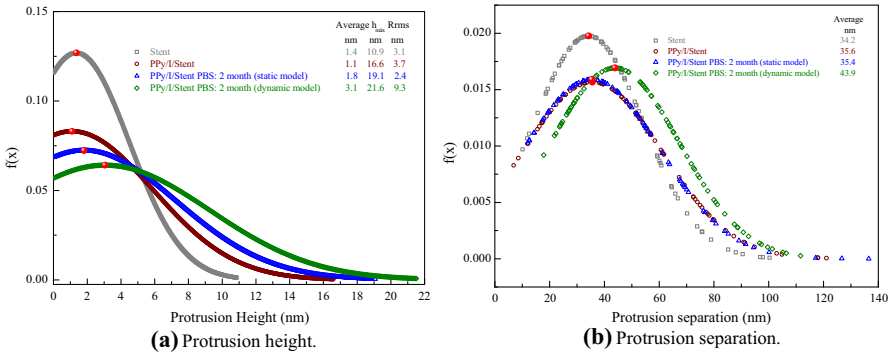


Fig. 7 Protrusion distribution of SS stent and PPy/I-coatings

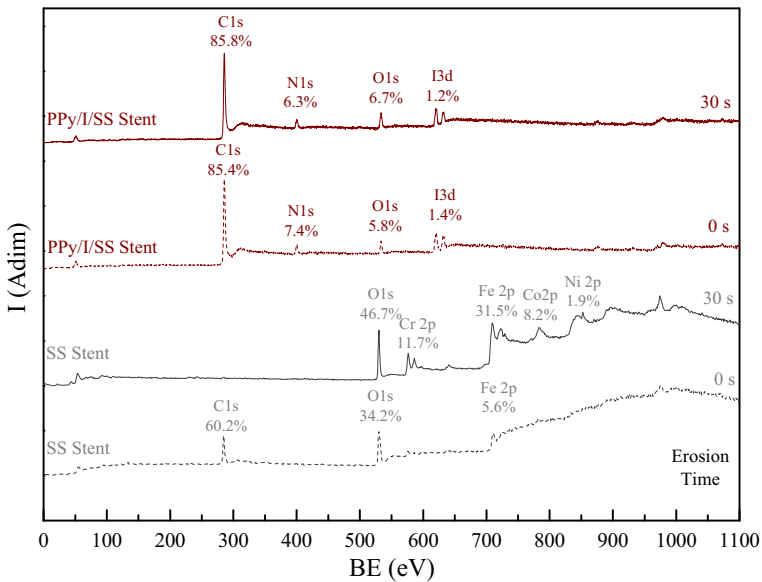


Fig. 8 XPS survey spectra of uncoated and coated SS stent with 0 and 30 s of plasma Ar erosion

oxidation after the synthesis. Another consideration is that the percentage of doping increased slightly with the erosion, which is an indication that iodine was combined in all the material.

These analyses indicate that the metallic surfaces have an organic layer that has to be removed before the synthesis of the PPy/I-coatings to bond the polymeric layer directly with the metal without intermediate layers, see the evolution of C1 s content in the samples before and after the erosion. This organic layer cannot be removed from the metallic surfaces with simple cleansing. Another observation is that oxidation is always present on the metallic and polymeric surfaces and has to be considered into the analyses.

Chemical states of the coating

The main superficial energetic atomic states of the PPy/I-coatings were studied through C1s, N1s, O1s and I3d orbitals. The detailed spectra were adjusted using Gaussian curves with full width at half maximum (FWHM) suggested in handbooks for advanced peak-fitting of monochromatic XPS spectra [17]. Figure 9a–d shows the C1s energetic distribution spectrum adjusted with five Gaussian curves with $FWHM = 1.0 \pm 0.1$ eV, the N1s spectrum adjusted with four curves with $FWHM = 1.2 \pm 0.1$ eV, the O1s spectrum adjusted with three Gaussian curves with $FWHM = 1.4 \pm 0.1$ eV, and the I3d 5/2 spectrum adjusted with two Gaussian curves with $FWHM = 1.3 \pm 0.1$ eV, respectively.

The graphs show the adjusted curves, represented by their maximum binding energy (BE), associated with at least one atomic chemical state and their percentage of participation. The atomic chemical states were assigned considering all possible bonds of each element, C = 4, N = 3, O = 2 and I = 1, and its atomic environment. The formation energy of the chemical states, annotated in blue inside the curves, is the sum of all atomic bond energies participating in the state [18, 19]. Some states could appertain to two curves depending on their formation energy, however, they will be discussed in the curve with the greatest participation.

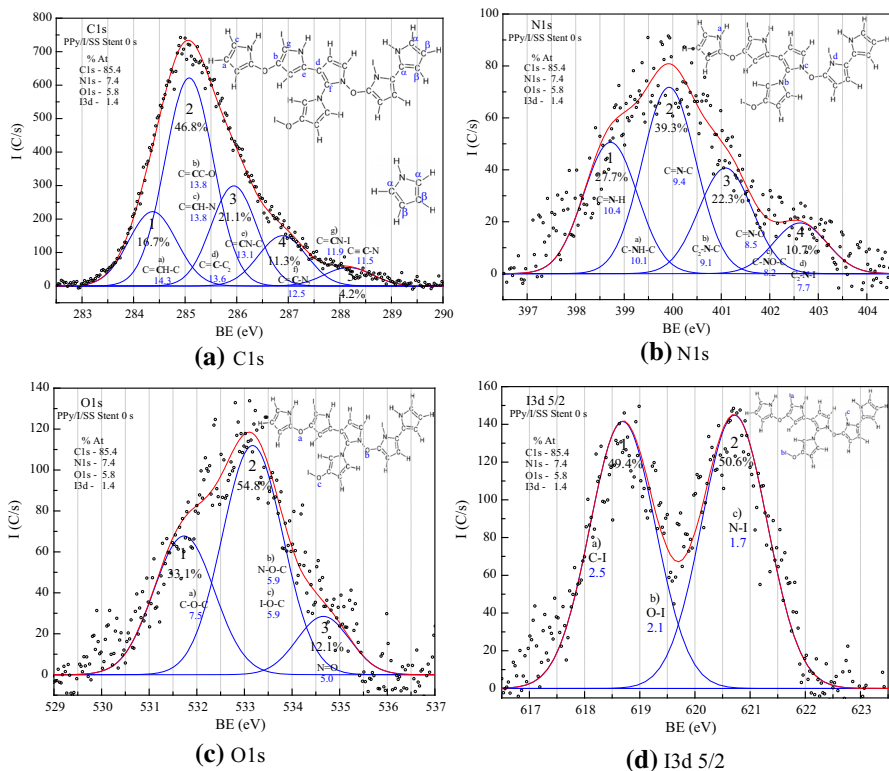


Fig. 9 Energetic distribution in the PPy/I/Stents of **a** C1s, **b** N1s, **c** O1s and **d** I3d 5/2 orbitals

The C1s energetic distribution of PPy/I-coatings is shown in Fig. 9a. The symmetry of pyrrole rings in this discussion is used to name the carbons next to the nitrogen atom as alpha carbons (α) and the others as beta carbons (β). Thus, the C=CH-C state in the first curve ($BE_{\max} = 284.4$ eV) corresponds to C in β positions in pyrrole rings that did not change or react during the polymerization. In a similar process, the second curve at 285.1 eV belongs partially to C in α positions (C=CH-N) that did not react. However, the second curve belongs also to an oxidized state (C=CC-O) of β Carbons due to the substitution of H for O atoms. Another chemical state can be found in this curve belonging to C in β positions (C=CC-C) joined with another C, probably with another pyrrole ring. The state at 285.9 eV in the third curve can be associated with the bond between rings in C α positions (C=CN-C) because of the dehydrogenation of those carbons. The fourth curve with maximum at 286.9 eV can be associated with the bonds between rings in C α positions and the N atom of another ring (C=C-N₂). C=CN-I in the fifth curve at 288.2 eV represents the interaction between C and iodine, although the energy belongs also to the most oxidized chemical state in the coatings, C \equiv C-N. Most of these states can be found in the molecular structure of Fig. 9a.

Figure 9b shows the chemical states of PPy/I-coatings considering N1 s orbitals. The first curve at 398.7 eV corresponds to N atoms in pyrrole rings that did not react during the polymerization, C-NH-C, and C=N-H is one mode of the state before considering the resonance in the rings. The states at 399.9 eV were associated with the interaction between two pyrrole rings through N and C atoms, C₂-N-C, and its resonance state, C=N-C, respectively. The state at 401.1 eV belongs to pyrrole rings that interact through N atoms with other rings through Oxygen bridges (C-NO-C) and its respective resonance configuration, C=N-O. The last state at 402.6 eV represents N atoms interacting with iodine in pyrrole rings, C₂-N-I.

O1s orbital curves of PPy/I-coatings are displayed in Fig. 9c. The states that could be assigned were C-O-C, N-O-C and I-O-C together, and N=O at 531.7, 533.2 and 534.7 eV, respectively. The first two curves have chemical states that may be associated with oxygen bridges between pyrrole rings, iodine or with fragments of molecules created due to the constant collisions in the plasma particles. The last state corresponds to more oxidized N atoms, N=O, maybe belonging to fragments of pyrrole rings.

Figure 9d presents the chemical states associated with I3d 5/2 orbitals. The first curve has a BE maximum at 618.7 eV and was assigned to C-I and O-I. The second curve has a BE maximum at 620.7 eV and was assigned to N-I.

In general terms, this analysis indicates that there are chemical states of pyrroles and fragments of them originated because of the collisions among electrons and ions accelerated by the electric field of the plasma. There are indicatives that all atoms in the pyrrole rings participated in the polymerization, not only alpha carbons, which are known to construct linear chains in the traditional chemical polymerizations. In the PPy coatings of stents, beta carbons were the most active. N atoms also participated actively in the chemical reactions.

Conclusions

Stents of stainless steel were conditioned and coated with PPy/I plasma to reduce the reaction rejection that these implants usually produce in the human circulatory system, however, this work was only devoted to the preparation of the coating and not to biological aspects. The results indicate that the Ar ions generated in the plasma collided with the surfaces eroding them, while the conditioning with H₂O₂ caused erosion and oxidation in which the polymeric layer grew with adherence to the metal following closely the superficial topology. In the superficial chemical structure of the PPy/I-coatings, there are chemical states of pyrrole rings in crosslinked configurations and other states that suggest some molecular fragmentation originated by the collisions of the monomers with the plasma particles, however, the major percentage of states corresponds to different unions between pyrrole rings with the active participation of all atoms in the chemical reactions which originated crosslinked networks. The resistance of the coatings was tested by immersing the coated stents for 2 months in flowing PBS solutions with pH and temperature similar to that of blood in the human system showing that they remained adhered to the surface without peeling or fractures on the coatings.

The average separation between protrusions in the stents was 34.2 nm, which increased slightly to 35.6 nm in the PPy/I-coatings. This means that the erosion did not change substantially the density of protrusions, but only changed their width and height. Particularly, the average height changed from 1.1 to 1.4 nm, before and after the coatings. The roughness in PPy/I-coatings was 3.7, 0.6 nm major than in the stents without coating, which give an idea about the average thickness of the coating on the protrusions. After 2 months, the immersion in PBS in the static model caused a roughness decrease from 3.7 to 2.4 nm, probably due to some dissolution of the external coating layer. The effect was different with the dynamic model, because the roughness increased from 3.7 to 9.3 nm as a consequence of the PBS flow erosion. The average separation between protrusions practically did not change in the static model, from 35.6 to 35.4 nm, however, in the dynamic model, the erosion increased the average separation between protrusions from 35.6 to 43.9 nm. Thus, the separation of protrusions was the most affected variable with the long-term PBS flow.

Acknowledgments The authors thank CONACYT in Mexico for the partial financial support to this work through the Project 154757 and for the doctor scholarship given to L.M. Gomez, to Jorge Perez for the support in the scanning electron microscopy, to Pavel López Carbajal for his service in the atomic force microscopy and to Arthesys, company of stent manufacturing (France), for the stent donation.

References

1. Xie D, Wan G, Maitz MF, Sun H, Huang N (2013) Deformation and corrosion behaviors of Ti–O film deposited 316L stainless steel by plasma immersion ion implantation and deposition. *Surf Coat Technol* 214:117–123. doi:[10.1016/j.surfcoat.2012.11.012](https://doi.org/10.1016/j.surfcoat.2012.11.012)
2. Oliva G, Espallargues M, Pons JMV (2004) Stents recubiertos de fármacos antiproliferativos: revisión sistemática del beneficio y estimación del impacto presupuestario. *Rev Esp Cardiol* 57:617–628. doi:[10.1157/13064187](https://doi.org/10.1157/13064187)

3. Cieslik M, Engvall K, Pan J, Kotarba A (2011) Silane–parylene coating for improving corrosion resistance of stainless steel 316L implant material. *Corros Sci* 53:296–301. doi:[10.1016/j.corsci.2010.09.034](https://doi.org/10.1016/j.corsci.2010.09.034)
4. Liu CL, Chu PK, Lin GQ, Qi M (2006) Anti-corrosion characteristics of nitride-coated AISI 316L stainless steel coronary stents. *Surf Coat Technol* 201:2802–2806. doi:[10.1016/j.surfcoat.2006.05.028](https://doi.org/10.1016/j.surfcoat.2006.05.028)
5. Vera R, Schreiber R, Grez P, Romero H (2014) The corrosion-inhibiting effect of polypyrrole films doped with p-toluene-sulfonate, benzene-sulfonate or dodecyl-sulfate anions, as coating on stainless steel in NaCl aqueous solutions. *Prog Org Coat* 77:853–858. doi:[10.1016/j.porgcoat.2014.01.015](https://doi.org/10.1016/j.porgcoat.2014.01.015)
6. Míndroiu M, Ungureanu C, Ion R, Pîrvu C (2013) The effect of deposition electrolyte on polypyrrole surface interaction with biological environment. *Appl Surf Sci* 276:401–410. doi:[10.1016/j.apsusc.2013.03.107](https://doi.org/10.1016/j.apsusc.2013.03.107)
7. Shaktawat V, Jain N, Saxena R, Saxena NS, Sharma K, Sharma TP (2006) Temperature dependence of electrical conduction in pure and doped polypyrrole. *Polym Bull* 57:535–543. doi:[10.1007/s00289-006-0580-9](https://doi.org/10.1007/s00289-006-0580-9)
8. Park DE, Chae HS, Choi HJ, Maity A (2015) Magnetite–polypyrrole core–shell structured microspheres and their dual stimuli-response under electric and magnetic fields. *J Mater Chem C* 3:3150–3158. doi:[10.1039/c5tc00007f](https://doi.org/10.1039/c5tc00007f)
9. Wang Y, Northwood DO (2008) Optimization of the polypyrrole-coating parameters for proton exchange membrane fuel cell bipolar plates using the Taguchi method. *J Power Source* 185:226–232. doi:[10.1016/j.jpowsour.2008.07.036](https://doi.org/10.1016/j.jpowsour.2008.07.036)
10. De Jesús C, Cruz GJ, Olayo MG, Gómez LM, López-Gracia OG, García-Rosales G, Ramírez-Santiago A, Ríos LC (2012) Coatings by plasmas of pyrrole on nitinol and stainless steel substrates. *Superficies y Vacío* 25:157–160
11. Khan W, Kapoor M, Kumar N (2007) Covalent attachment of proteins to functionalized polypyrrole-coated metallic surfaces for improved biocompatibility. *Acta Biomater* 3:541–549. doi:[10.1016/j.actbio.2007.01.006](https://doi.org/10.1016/j.actbio.2007.01.006)
12. Myung SW, Choi HS (2006) Chemical structure and surface morphology of plasma polymerized-allylamine film. *Korean J Chem Eng* 23:505–511. doi:[10.1007/BF02706757](https://doi.org/10.1007/BF02706757)
13. Airoudj A, Schrodj G, Vallat M-F, Fioux P, Roucoules V (2011) Influence of plasma duty cycle during plasma polymerization in adhesive bonding. *Int J Adhes Adhes* 31:498–506. doi:[10.1016/j.ijadhadh.2011.05.003](https://doi.org/10.1016/j.ijadhadh.2011.05.003)
14. Kane JW, Sternheim MM (2007) Física. Reverte, España
15. Cruz GJ, Olayo MG, Salgado H, Díaz A, Ríos LC, Olayo R, Morales J, Mondragón R, Morales A (2010) Contributions to the advancement of science and technology in Mexico. Strategy for the treatment of spinal cord injuries after complete section using polymeric implants synthesized by plasma. ININ, México
16. Deuse T, Hua X, Wang D, Maegdefessel L, Heeren J, Scheja L, Bolaños JP, Rakovic A, Spin JM, Stubbendorff M, Ikeno F, Länger F, Zeller T, Schulte-Uentrop L, Stoehr A, Itagaki R, Haddad F, Eschenhagen T, Blankenberg S, Kiefmann R, Reichenspurner H, Velden J, Klein C, Yeung A, Robbins RC, Tsao PS, Schrepfer S (2014) Dichloroacetate prevents restenosis in preclinical animal models of vessel injury. *Nature* 509:641–644. doi:[10.1038/nature13232](https://doi.org/10.1038/nature13232)
17. Crist BV (1998) Advanced peak-fitting of monochromatic XPS spectra. *J Surf Anal* 4:428–434
18. Cotton FA, Wilkinson G (1980) Química inorgánica avanzada. Limusa, Mexico
19. Dean JA (1999) Langés handbook of chemistry. McGraw-Hill, New York